Robert Cell-Based Optical Delay Elements for White Cell True-Time Delay Devices

Yu Shi and Betty Lise Anderson, *Senior Member, IEEE*

***Abstract*—A low-loss and compact optical delay element is devised to be integrated into existing White cell-based true-time delay systems. The delay element is based on a multiple-bounce cell that consists of simple optical components, which was initially described by Claude Robert for spectroscopy. We hereby provide a comprehensive analysis of the Robert cell and propose that it can be modified in a number of ways to produce discrete and variable time delays up to hundreds of ns. The Robert cell show appealing traits compared to traditional optical delay devices because it relies on reflections within a system of mirrors to produce time delays, and this mechanism reduces the physical size and optical losses compared to traditional approaches for long delays. We also illustrate how modified Robert cells can be designed such that they can be compatibly combined with White cell-based true-time delay systems.**

***Index Terms*—Phased arrays, optical delay lines, optical signal processing, optics.**

I. Introduction

OPTICAL time delays are important for such applications as steering phased array antennas, tapped or programmable delay lines for matched filtering, optical correlation, and signal processing, and potentially even optical buffering if long enough delays can be produced without excessive loss and cost. In this work, we propose new methods for obtaining long and variable optical delays that can be used for the systems mentioned above, and we provide a detailed examination on how the new device can be combined with existing optical true-time delay (TTD) systems.

In the example of phased-array antennas, they are made up of a series of independent, small-element antennas that jointly produce a concentrated electromagnetic beam propagating at desired directions [1]. To control their emission and reception directions, each antenna element must be phase-shifted or time-delayed by a precise amount. For broadband radar systems, TTD must be used because they prevent beam squint, where different frequencies travel in different directions [2]. Optical TTD systems are attractive because of their low weight and high degree of flexibility, and more recently, a free-space approach to optical TTD was demonstrated based on the White cell, which has the lowest size, weight, and power of any known system [3]. The longest delay in that system was 25 ns; in this work, we describe ways with which we can achieve much longer delays.

One type of White cell-based TTD system is the binary White cell [4], which consists of two White cells that share a common micro-electro-mechanical system (MEMS) mirror arrays. One White cell acts as a switching engine and the other includes optical delay elements. Traditional delay elements include dielectric blocks, lens trains, and optical fibers. Dielectric blocks are only appropriate for very short delays on the order of picoseconds, because as the blocks get longer they begin to block the beams circulating in the White cell. Larger delays implemented in lens trains can become prohibitively long and require many discrete lenses with precise alignment, which is a very tedious and difficult process. Lens trains may be used for delays up to around 25 ns. Up to now, achieving longer delays has required fibers, which also introduce alignment issues, coupling losses, and dispersion [5].

To reduce the loss and physical sizes of the delay elements, we propose a free-space multipass reflection system that can be integrated into a White cell-based TTD system. We adopt the Robert cell [6], which is already low-loss and compact, as the basis for our new delay elements, and we design modifications that make it a delay element compatible with the binary White cell architecture.

We begin our discussion in Section II by briefly reviewing the principles of operations for both the White cell and the binary cell. In Section III, we present an overview of the Robert cell and provide analyses and derivations of its properties. Section IV contains a detailed description of our modifications of the Robert cell and how we can incorporate them into a binary cell system. We finish our discussion in Section V, which includes summaries and conclusions.

II. Binary White-Cell-Based TTD Device

A. White Cell

The White cell [7] consists of three spherical mirrors A, B, C with the same radii of curvature. Shown in Fig. 1, mirrors A and B are placed on the same side, and they are separated from mirror C by a distance equal to the radius of curvature. The center of curvatures of mirrors A and B are adjusted such that they are a small distance apart from each other. When an array of focused beams enters the White cell through the input turning mirror, the spots are refocused by either mirror A or B,

Manuscript received September 18, 2012; revised December 18, 2012; accepted December 19, 2012. Date of publication December 25, 2012; date of current version February 06, 2013. This work was supported in part by the U.S. Department of Commerce under Grant BS123456

The authors are with the Electrical and Computer Engineering Department, The Ohio State University, Columbus, OH 43201 USA (e-mail: shi.110@osu.edu).

Color versions of one or more of the figures in this paper are available online at http://ieeexplore.ieee.org.

Color versions of one or more of the figures in this paper are available online at http://ieeexplore.ieee.org.

Digital Object Identifier 10.1109/JLT.2012.2236537

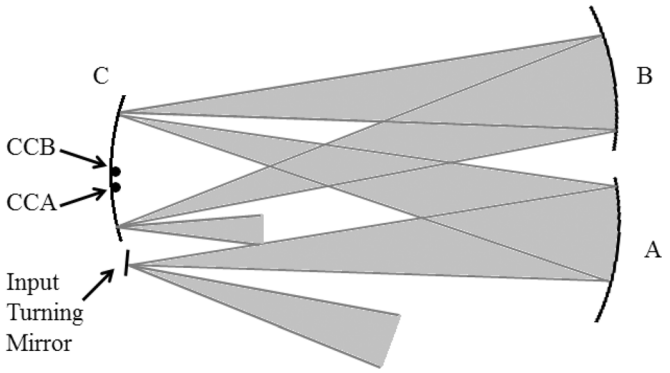

Fig. 1. Structure of a White cell. A focused beam enters the system through the input turning mirror, and mirrors A and B reimage the beam onto mirror C. The input can be a single spot or an array.

forming a new array of imaged and non-overlapping spots on mirror C.

B. Binary Cell

The binary White cell is a specific adaptation that can be conceived as essentially two independent White cells that share a MEMS micromirror array, which can switch the beams from one cell to the other.

The structure of a binary White cell is shown in Fig. 2(a), which contains cells AB and CD. The spot patterns are shown in Fig. 2(b). When a row of focused beams enters the system via the input turning mirror, the beams diverge and hit mirror B, which re-images the beams onto the first row of pixels on the MEMS. The MEMS can now be used as the switching engine. For each cycle of operation, for those MEMS pixels that are flat, the corresponding beams travel to mirror A and get imaged back onto the first row of the auxiliary mirror. The auxiliary mirror reflects the beams back onto mirror B, which focuses the beams onto the second row of the MEMS. On the other hand, if some of the MEMS pixels are tilted, then the selected beams reach mirror C, which focuses those beams into the first row of the delay plane. The outputs of the delay plane hit mirror D and are also focused back onto the second row of the MEMS [4].

During each cycle of operation, the null cell AB adds no excess delay to the beams, whereas the delay plane typically adds a time delay that is proportional to 2^n, where n is the cycle of operation. After n cycles, the binary cell can produce a maximum time delay that is proportional to $2^{n+1} - 1$ [4].

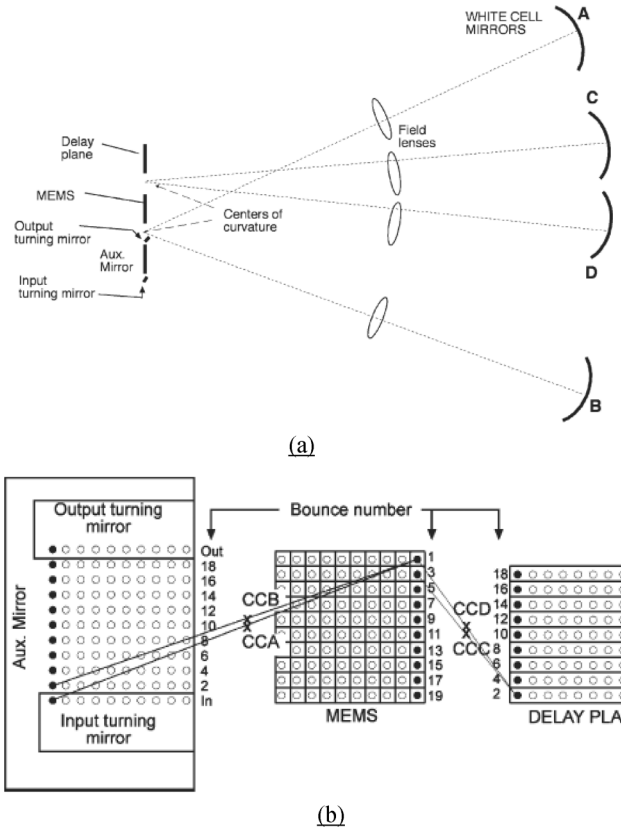

Fig. 2. (a) Structure and spot patterns of a binary White cell system. (b) Spot patterns created from a binary White cell [4].

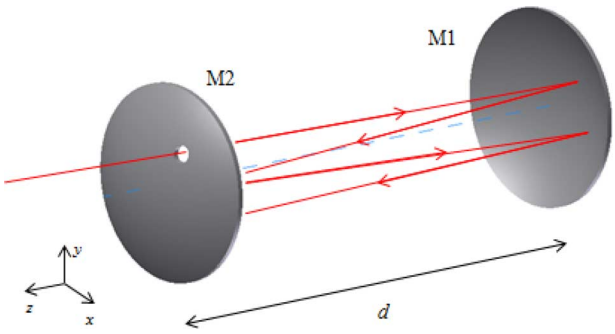

Fig. 3. Structure of a Herriott cell. M1 and M2 are both spherical mirrors, separated by a distance d.

III. Properties of the Robert Cell

Next, we discuss the Robert cell and how it can be incorporated into a binary-style White cell TTD device. The Robert cell has a very similar structure compared to the well-known Herriott cell [8]. In fact, both the White cell and the Heririott cell are special cases of the Robert cell [6]. We will first examine the properties of the Herriott cell before analyzing the Robert cell.

A. The Herriott Cell

The Herriott cell (Fig. 3) consists of two spherical mirrors, M1 and M2, placed on the same optical axis facing each other [8]. A beam can enter from an aperture on mirror M2, and it reflects within the cell and exits though the same aperture. As the beam circulates, it forms a series of spots on the mirrors, which we analyze next.

1) Ray Matrix: The spot patterns of the Herriott cell can be derived using paraxial ray matrices. Each ray can be described by a 4×1 ray vector, $\mathbf{r} = [x, S_x, y, S_y]^{\mathrm{T}}$, where x and y are the positions of the rays at a specified plane, and S_x and S_y are the corresponding slopes of the rays. In a three dimensional space, each optical component or ray operation can be described by a 4×4 matrix. For a Herriott cell, the operations on a ray comes either from a spherical mirror with a radius of curvature R or

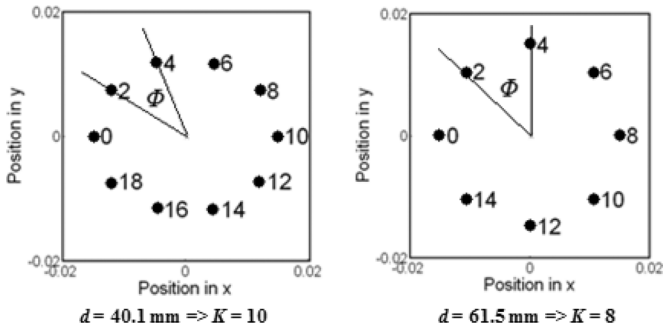

Fig. 4. Herriott cell's spot patterns. The indices next to the spots represent the number of reflections that the beam has experienced. When the distance between the mirrors is increased, the angle between successive reflections increase, and thus the period K becomes smaller. Mirror parameters: $R_1 = 420$ mm, $R_2 = \infty$.

from traveling a distance d, and their matrix representations are $\mathbf{T}(R)$ and $\mathbf{T}(d)$, respectively [9], given as

$$\mathbf{T}(R) = \begin{pmatrix} 1 & 0 & 0 & 0 \\ -2/R & 1 & 0 & 0 \\ 0 & 0 & 1 & 0 \\ 0 & 0 & -2/R & 1 \end{pmatrix} \tag{1}$$

$$\mathbf{T}(d) = \begin{pmatrix} 1 & d & 0 & 0 \\ 0 & 1 & 0 & 0 \\ 0 & 0 & 1 & d \\ 0 & 0 & 0 & 1 \end{pmatrix}. \tag{2}$$

The operation of the Herriott cell on a ray is periodic because in each cycle, the ray first travels a distance d, gets reflected by mirror M1, travels another distance d, and hits mirror M2. Thus, each cycle of operation can be represented by [9]

$$\mathbf{r}_{n+1} = \mathbf{T}(R_2) * \mathbf{T}(d) * \mathbf{T}(R_1) * \mathbf{T}(d) * \mathbf{r}_n = \mathbf{T} * \mathbf{r}_n. \tag{3}$$

Given the initial ray vector $\mathbf{r}_0$, the ray vector after n cycles becomes [9]

$$\mathbf{r}_n = \mathbf{T}^n * \mathbf{r}_0. \tag{4}$$

Shown in Fig. 4, the Herriott cell spot patterns form elliptical shapes, and the angle between two successive spots is given by $\Phi = 2\alpha$, where [6], [8]

$$\cos(\alpha) = \sqrt{\left(1 - \frac{d}{R_1}\right)\left(1 - \frac{d}{R_2}\right)}. \tag{5}$$

When Φ satisfies $\Phi * K = 360°$, where K is an integer, the spot pattern becomes periodic in that it repeats itself after K cycles. At the Kth cycle, the beam exits the system through the same aperture from which it entered.

2) Difference Equations: A mathematical approach that provides more insight to the Herriott cell system is via the difference equations analysis. Knowing the transfer matrix $\mathbf{T}$ for each cycle and given the current state ray vector $\mathbf{r}_n$, we can calculate the next state ray vector, $\mathbf{r}_{n+1}$, according to (3) using matrix multiplication, which results in a system of four coupled equations. Due to symmetry in the x and y directions, we only have to show the equations in the x direction because the equations in the y direction assume the same form of

$$x_{n+1} = A\, x_n + B\, (S_x)_n \tag{6}$$

$$(S_x)_{n+1} = C\, x_n + D (S_x)_n \tag{7}$$

where, from (1), (2), and (3), we have

$$\begin{aligned} A &= 1 - \frac{2d}{R_1} \\ B &= 2d - \frac{2d^2}{R_1} \\ C &= -\frac{2}{R_1} - \frac{2}{R_2} + \frac{4d}{R_1 R_2} \\ D &= 1 - \frac{4d}{R_2} - \frac{2d}{R_1} + \frac{4d^2}{R_1 R_2}. \end{aligned} \tag{8}$$

These equations can be solved by combining the equations into a single-variable second order difference equation, and then guessing a homogeneous solution $x_n = x_0 * h^n$, where x_0 is the initial input location and h is a complex number. The final forms of their solutions are

$$x_n = x_0 \cos(\Phi * n) + k_2 \sin(\Phi * n) \tag{9}$$

$$(S_x)_n = (S_x)_0 \cos(\Phi * n) + p_2 \sin(\Phi * n) \tag{10}$$

where k_2 and p_2 are determined by the initial conditions of position and slope, and

$$\cos\left(\frac{\Phi}{2}\right) = \sqrt{\left(1 - \frac{d}{R_1}\right)\left(1 - \frac{d}{R_2}\right)}. \tag{11}$$

Thus, the difference equation approach yields the same result obtained by Herriott and Robert in (5). We will also use this technique in section B for the Robert cell spot pattern analysis.

Equations (9) and (10) demonstrate that the solutions for both the positions and slopes of the spot patterns are parametric sine and cosine equations, implying that the evolution of both the ray positions and their slopes follow elliptical trajectories.

B. The Robert Cell

The structure of the Robert cell shown in Fig. 5(a) is almost identical to that of a Herriott cell. The only difference is that the mirror on the input side, M2, is split in half along the x-axis. While the top half of the mirror (M2+) is fixed, the lower half (M2−) is allowed to rotate by an arbitrary angle θ about the y-axis [6].

The mathematical formulism for the Robert cell system is largely similar to that of the Herriott cell, and the ray matrix and difference equation techniques can both be applied.

1) Ray Matrix: When a ray enters the Robert cell system, it bounces either between M1 and M2+ when $y > 0$ or between M1 and M2− when $y < 0$. When M2+ is struck, the cell acts as if it was a normal Herriott cell, and the same ray matrix shown in (1) can be applied. However, if the ray hits M2− tilted at an angle θ, the slope in the x direction will be further deflected

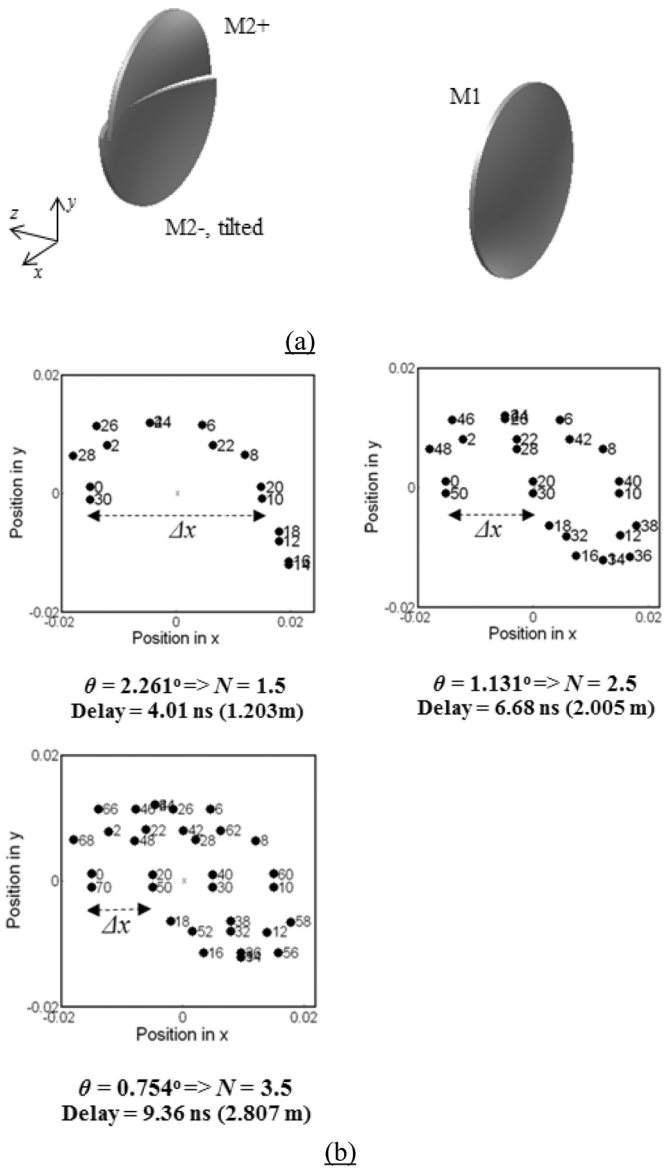

Fig. 5. (a) Structure of a Robert Cell. (b) Spot patterns formed by the Robert cell under different angles of rotation. Cell parameters: $R_1 = 420$ mm, $R_2 = \infty$, $d = 40.1$ mm.

by $2\tan(\theta)$. To account for this new term, the ray matrix for a spherical mirror in (1) is modified to be

$$\mathbf{T}(R_2-) = \begin{pmatrix} 1 & 0 & 0 & 0 \\ -\frac{2}{R} & 1+\frac{2\tan(\theta)}{S_x} & 0 & 0 \\ 0 & 0 & 1 & 0 \\ 0 & 0 & -\frac{2}{R} & 1 \end{pmatrix} \quad (12)$$

Now, the next state ray vector can be computed as:

$$y > 0: \quad \mathbf{r}_{n+1} = \mathbf{T}(R_2+) * \mathbf{T}(d) * \mathbf{T}(R_1) * \mathbf{T}(d) * \mathbf{r}_n = \mathbf{T}_+ * \mathbf{r}_n \quad (13)$$

$$y < 0: \quad \mathbf{r}_{n+1} = \mathbf{T}(R_2-) * \mathbf{T}(d) * \mathbf{T}(R_1) * \mathbf{T}(d) * \mathbf{r}_n = \mathbf{T}_- * \mathbf{r}_n. \quad (14)$$

Some examples of the Robert cell spot patterns are shown in Fig. 5(b), where the cell parameters are chosen such that they would produce patterns whose periodicity is 10 if they were used in the Herriott cell. These patterns show that as predicted, the y-positions of the spots are still periodic with a periodicity $K = 10$. However, for every K cycles, when the y-position returns to its initial value, the spots' x-positions shift linearly by Δx, a quantity that decreases as θ decreases. The spots seem to swirl toward the center of the mirrors; upon reaching the center, they start to swirl out again. It is then appropriate to define every K cycles of the Robert cell to be one "swirl," and multiple swirls are denoted by N swirls.

The results in Fig. 5(b) also demonstrate that the Robert cell has the potential to be used as a compact delay element. For example, with the mirror separation of merely $d = 40.1$ mm, the beam traveled for 2.807 m in the case where $N = 3.5$ and $K = 10$, which corresponds to a time delay of 9.36 ns. To achieve the same delay with the lens train requires the system to be 1.4 m long and may require many lenses that have different focal lengths depending on the spot size and the number of spots. Thus, the Robert cell shows great promise in shrinking the physical dimensions of the true-time delay system.

On top of that, the amount of loss corresponding to the Robert cell is expected to be low because of the use of reflection. High-reflectivity coating on mirrors can be made better than anti-reflection coatings on lenses, and lenses have two surfaces instead of one. If the device is built with a dielectric mirror that has a reflectivity of 0.999, the amount of loss produced after 70 reflections in Fig. 6 (a time delay of 9.36 ns) would merely be $0.999^{70} = 0.93 = -0.304$ dB.

2) Difference Equations: Recall that the lower mirror's angle rotation θ about the y-axis has no effect on the position or slope in the y direction. Therefore, (9) and (10) still hold for y and S_y.

The difference equation analysis in the x-direction, however, must be split up into two scenarios. When the ray hits M2+ and matrix $\mathbf{T}_+$ is applied to the ray vector, we can readily use (9) and (10). Nonetheless, if the ray hits M2− and $\mathbf{T}_-$ is applied, S_x will be further deflected by $2\tan(\theta)$, resulting in the following coupled difference equations:

$$x_{n+1} = Ax_n + B(S_x)_n \quad (15)$$

$$(S_x)_{n+1} = Cx_n + D(S_x)_n + 2\tan(\theta) \quad (16)$$

where A, B, C, D inherit the same form as they did in (8).

When these equations are solved using the same procedures as we used in solving the Herriott cell, we obtain solutions that contain a homogeneous part composed of sinusoidal functions and a particular part that varies linearly with respect to $\tan(\theta)$. The final forms of these equations are as follows:

$$x_n = k_1\cos(\Phi * n) + k_2\sin(\Phi * n) + \frac{B}{1-b}\tan(\theta) \quad (17)$$

$$(S_x)_n = p_1\cos(\Phi * n) + p_2\sin(\Phi * n) + \frac{(1-A)}{(1-b)}\tan(\theta) \quad (18)$$

where $b = (A+D)/2$. The values k_1, k_2, p_1, and p_2 are determined by the initial conditions $[x_0, (S_x)_0]$ and cell parameters, and A, B, Φ are all identical to their forms in (8) and (11).

3) Interpretation of the Difference Equation Solutions: The interpretation of the Robert cell solutions is not a trivial task, because in different cycles, the ray may strike M2+ or M2−,

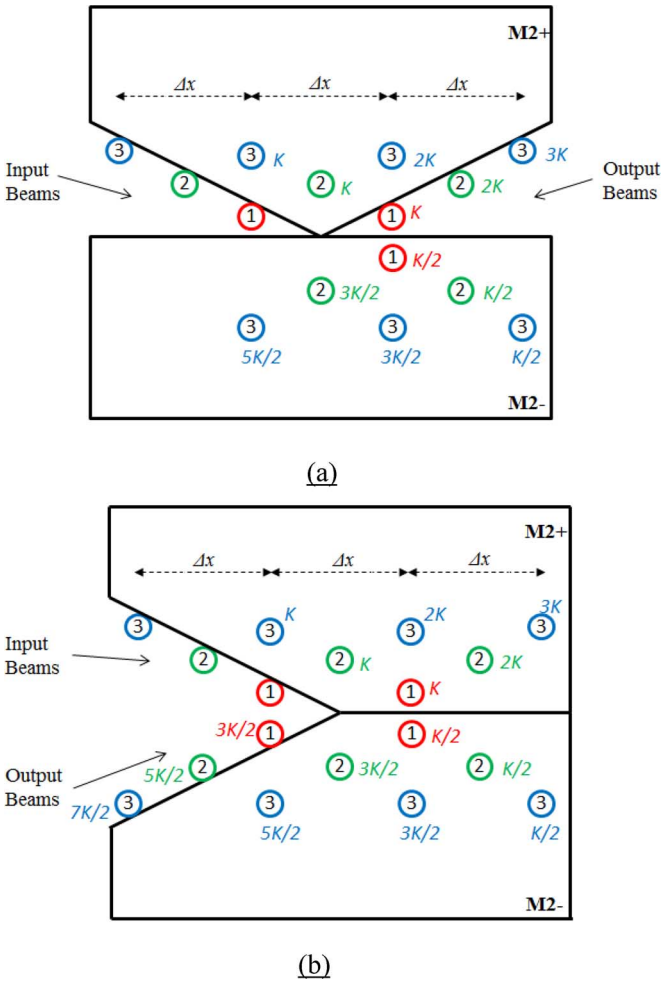

Fig. 6. Front view of the Robert cell designs that allow beams to enter from different input locations to achieve different time delays. (a) Allows beams to exit after full N swirls, whereas (b) allows beams to exit after $N + 1/2$ swirls.

each of which corresponds to a different solution. The result of this is the analysis of piece-wise discrete parametric equations in the x and y directions. To simplify our analysis, we choose to examine the case where Φ satisfies the periodicity condition, where $360/\Phi = K =$ the period. We further require K to be an even integer.

a) Solutions in the y-Direction: In the y-direction, the position and slope are independent of the rotational angle θ, so the sinusoidal solutions shown in (9) and (10) can be used regardless of whether the ray hits M2+ or M2−. Thus, for every K cycles (or full N swirls), the position and slope in y returns to their input values; for an extra $K/2$ cycles (or at $N + 1/2$ swirls), the sinusoidal nature of the solutions implies that the position and slope in y would simply be the negative of the input values.

b) Solutions in the x-Direction: The solutions in the x-direction require a more systematic treatment. When the ray travels onto M2+, we need to use (9) and (10), whereas a ray that lands on M2− would need solutions in (17) and (18). Because the solutions for both the position and slope take on the same form, we can start analyzing the behavior of the x-position and obtain the same insight for the x-slope.

TABLE I
ITERATIVE ANALYSIS OF THE RAY POSITION FOR EVERY HALF SWIRL

N (swirls)	Mirror Hit	Current x-position x_n	Current Equation	g_1	g_2
0	M2+	$-x_0$	(20)	$-x_0$	/
1/2	M2-	x_0	(21)	/	$-x_0 + \delta$
1	M2+	$-x_0 + 2\delta$	(20)	$-x_0 + 2\delta$	/
3/2	M2-	$x_0 - 2\delta$	(21)	/	$-x_0 + 3\delta$
2	M2+	$-x_0 + 4\delta$	(20)	$-x_0 + 4\delta$	/
5/2	M2-	$x_0 - 4\delta$	(21)	/	$-x_0 + 5\delta$
3	M2+	$-x_0 + 6\delta$	(20)	$-x_0 + 6\delta$	/

Assume that a ray is sent into the system with $x = -x_o$, $y > 0$, and $S_y > 0$ so that it begins its operations on M2+. To further simplify our discussion, we choose an input slope S_x such that it eliminates the sine term. If we restrict our analysis to multiples of 1/2 swirls, the cosine term merely alternates being -1 or 1, and solutions in the x-position can now be described as

$$y > 0 \quad x_n = g_1 * (-1)^{2N} \tag{19}$$

$$y < 0 \quad x_n = g_2 * (-1)^{2N} + \delta \tag{20}$$

where g_1 and g_2 are arbitrary constants that depend on the current ray position, N denotes the number of swirls and is restricted to be multiples of 1/2, and $\delta = [B/(1-b)\tan(\theta)]$, which represents the linear term in (17).

We can now iteratively analyze the ray position for every half of a swirl as presented in Table I. For every half swirl, we need to first determine which mirror the ray hits and what equation we will apply, and then we need to update the values of g_1 or g_2 according to the current ray position. This analysis demonstrates that for each swirl, the ray's position is linearly shifted by $\Delta x = 2\delta$. This is significant because we can control the number of swirls (and thereby the time delay) by adjusting the angle of rotation for M2−; the smaller the angle, smaller the Δx, and hence the more the swirls and the longer the time delay. Table I also shows that an addition of 1/2 a swirl reflects the positions of the ray across the origin, thus flipping their signs.

The analysis for the x-slope yields similar results. For each full swirl, the Robert cell adds on $\Delta S_x = 2((1-A))/((1-b))\tan(\theta)$ to the previous slope value. Usually, ΔS_x is a very small quantity on the order of 0.01. Any additional 1/2 swirl flips the sign of the previous slope value.

4) Robert Cell Properties: The implications of the mathematical solutions can be summarized into the following properties of a Robert cell system with N swirls.

Property 1, Position in y: For $n = N * K$ cycles, the position in y is the same as that of the input, $y_n = y_0$.

Property 2, Slope in y: For $n = N * K$ cycles, the slope in y is the same as that of the input, $(S_y)_n = (S_y)_0$.

Property 3, Position in x: For every swirl, the position in x shifts by Δx that is calculated as

$$\Delta x = 2 * \frac{B}{1-b}\tan(\theta). \tag{21}$$

After N swirls, the ray's position in x becomes $x_n = x_0 + N * \Delta x$.

Property 4, Slope in x: For every swirl, the slope in x shifts by a small quantity ΔS_x calculated as

$$\Delta S_x = 2 * \frac{(1-A)}{(1-b)} \tan(\theta). \tag{22}$$

After N swirls, the ray's slope becomes $(S_x)_n = (S_x)_0 + N * \Delta S_x$.

Property 5, Additional 1/2 Swirl: For any additional 1/2 swirl, the ray's positions and slopes simply are simply the negative of their previous states.

Of all the properties of the Robert cell, Property 4 is the most unusual and intriguing. Unlike many commonly used optical components, the device adds a constant angle in the x-direction to an input ray regardless of the input angle. This is different from a mirror or a prism, the former of which reflects a beam at the same angle as the angle of incidence, and the latter of which rotates the beam's angle by a quantity determined by the input angle.

C. White Cell's Relationships to the Robert Cell

As mentioned before, the White cell and the Herriott cell can be considered as special cases of the Robert cell [6]. In a Herriott cell, when M2 is split in half, it creates a three-mirror system, where M2+ and M2− share the same center of curvature. However, when M2− is rotated by a small angle, its center of curvature (CC) is shifted slightly from that of M2+, much similar to the way the objective mirrors in a White cell have slightly different CCs [6]. Furthermore, the spot patterns of the Robert cell and the White cell have analogous characteristics. In each cycle, the White cell produces spots that are in rows or columns on mirror C, whereas Fig. 5(b) shows that the Robert cell creates rows of spots for every $K/2$ cycles. Furthermore, the Robert cell's mathematical formalism suggests that if $R_1 = R_2 = d$, rows of spots can be produced during each cycle without any intermediate spots. Therefore, the White cell is a case of the Robert cell whose radii of curvatures for all of the mirrors are equal to their distance of separation [6].

D. Imaging Conditions

To practically implement a delay element into a White cell-based system, the delay device should allow the input of a set of beams focused to an array of spots, and the delay element's output beams should also be focused. For a Robert cell system, there are three degrees of freedom with parameters R_1, R_2, and d. These parameters must be chosen to satisfy the periodicity constraint in (5) and the input-output focusing constraint. On top of that, one can specify a distance d to obtain the desired time delay increment. Therefore, we have three variables and three equations to solve.

For the output beam to image, we chose to design Robert cells that focus the beams for every 1/2 swirl, or $K/2$ cycles, in which case the beam will also be focused at the output after N or $N + 1/2$ swirls.

We obtain the equation that satisfies imaging using the ray matrix analysis. For a general ray transfer matrix $\mathbf{H} = \begin{pmatrix} A & B \\ C & D \end{pmatrix}$, if $B = 0$, then the imaging condition is satisfied. Note that the imaging condition for the Robert cell is the same as that of the Herriott cell provided that the angle of rotation θ is small, so we can work with (4) to determine the transfer matrix after $K/2$ cycles by extracting the B value of the matrix $\mathbf{T}^{K/2}$.

The B value is a function of R_1, R_2, and d, and it is typically a complicated nonlinear equation. Combined with the periodicity constraint, the values of R_1, R_2, and d are best solved numerically. If we want a cell to have a time delay of 2 ns per swirl with a periodicity of $K = 8$, we can set the distance between the mirrors to be $d = 375$ mm. To satisfy both the imaging and the periodicity constraint, the radii of focus are calculated to be $R_1 = 258$ mm and $R_2 = 26.7 \times 10^3$ mm $\approx \infty$.

IV. Modifications to the Robert Cell and Their Integration Into the White Cell

A. Variable Time Delays Within a Single Cell

The first set of modifications to the Robert cell is that M2+ and M2− can be shaped such that the device allows the rays to enter and exit from different positions whose x-coordinates are multiples of $\Delta x/2$. Each input location also corresponds to a different amount of delay. The schematics of these two designs are displayed in Fig. 6, which shows three different input locations that are labeled with different colors. All intermediate spots are hidden except for those that have undergone multiples of $K/2$ cycles (or half a swirl), and they are indexed in terms of K with their corresponding colors. Part (a) shows a design that allows the beam to make a full N swirls, whereas the design in part (b) allows the beam to make $N + 1/2$ swirls. By cutting off the edges of mirrors M2+ and/or M2−, only the input and output locations miss the mirrors to communicate with the space outside and all intermediate reflections are contained within the cell. For input locations farther from the center of the device, the ray experiences more swirls and thus carries a longer time delay.

The input and output conditions are different for these two schematics. For the device shown in Fig. 6(a), the Cartesian coordinate of their input and output relationships are

$$\begin{aligned} x_{\text{out}} &= -x_{\text{in}} \\ y_{\text{out}} &= y_{\text{in}} \\ (S_x)_{\text{out}} &= (S_x)_{\text{in}} + \gamma_1 \\ (S_y)_{\text{out}} &= (S_y)_{\text{in}}. \end{aligned} \tag{21}$$

Equation (21) can also be represented pictorially as shown in Fig. 7(a). For a Robert cell that performs N swirls, the input beam position is reflected about the y-axis. The output beam slopes relate to the input slopes as follows: In the y direction, the slope of return equals to that of incidence, just as a mirror; in the x direction, the slope is also similar to a beam striking a mirror, except the slope in the x-direction is additionally rotated by a small quantity γ_1, which is specified by the angle offset due to the tilt of M2−.

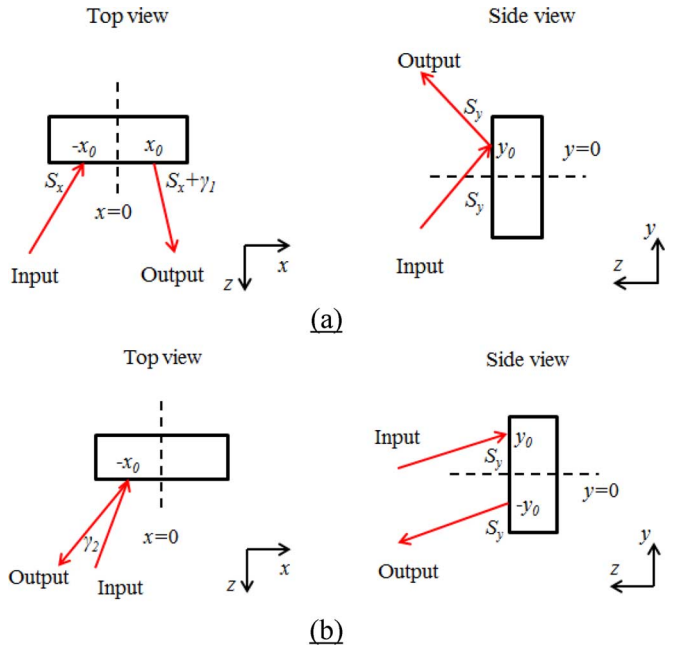

Fig. 7. Top- and side-view illustrations of the Robert cell input and output relationships. (a) Device that performs full N swirls. (b) Device that performs $N + 1/2$ swirls.

Whereas, for device in Fig. 6(b), we have

$$\begin{aligned} x_{\text{out}} &= x_{\text{in}} \\ y_{\text{out}} &= -y_{\text{in}} \\ (S_x)_{\text{out}} &= -(S_x)_{\text{in}} + \gamma_2 \\ (S_y)_{\text{out}} &= -(S_y)_{\text{in}}. \end{aligned} \tag{22}$$

The relationships in (22) are also depicted in Fig. 7(b), which shows that for a Robert cell that performs $N + 1/2$ swirls, the input position is reflected across the x-axis. The output beam travels in a direction that is almost anti-parallel to the input beam, except that the slope in the x-direction is rotated by γ_2.

B. Robert Cell Coupling

To create much longer time delays, two Robert cells can be coupled using a spherical mirror. For ultra-long delays, two of the same cells shown in Fig. 6(b) are used as shown in Fig. 8. When a beam first enters cell 1, it exits after $N + 1/2$ swirls and impinges onto the auxiliary spherical mirror $\mathrm{M_A}$. $\mathrm{M_A}$'s center of curvature is positioned such that it reflects the output of the first Robert cell onto the input of cell 2, whose output returns back into the input of cell 1 via $\mathrm{M_A}$ at the new location. The beam is delayed further, and returns to the second Robert cell again at a new location. Thus, the input beam bounces back and forth between these two cells some number of times, accumulating very long delays. Due to the small angular rotation γ_2 in (22), the ray is slowly rotated to the left for every time it enters a cell, and the beam will eventually miss mirror $\mathrm{M_A}$ and exit from the output position of cell 2.

A single Robert cell that has a mirror separation of a few centimeters can achieve a delay on the order of 10 to 20 ns.

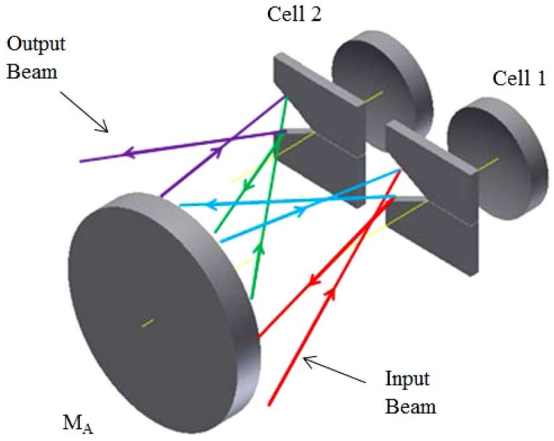

Fig. 8. Coupled Robert cell system. Mirror $\mathrm{M_A}$ is placed such that the output of one cell is reflected to the input of the other cell.

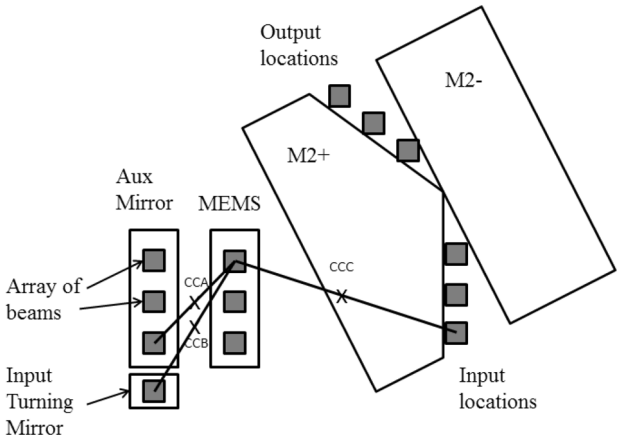

Fig. 9. Employing a single modified Robert cell as a delay plane for the Binary cell. Unfortunately, a line connecting the output locations is not parallel to a line connecting the input locations.

With the coupled Robert cell, however, delays on the order of 100 ns can be easily obtained.

C. Robert Cell as a Delay Element for the Binary Cell

As discussed in Section II, the binary White cell needs a delay plane whose amount of delay varies with the input position. Thus, both of the Robert cell configurations in Fig. 6 are compatible to this requirement. We choose to adopt the design in Fig. 6(a) because all of its swirls are full integers, making its analysis easier. Because the input positions of the Robert cell are slanted, the cell needs to be rotated such that a line joining the input locations is vertical as shown in Fig. 9, so that it matches the arrangement of the light beams on the MEMS.

Now, however, the line joining the output beam locations is not parallel to the line of input beam locations. Normally in the White cell, the beams leaving the delay plane are re-imaged onto the MEMS by a single objective mirror, e.g., Mirror D in Fig. 2. The output beams from the Robert cell are on a diagonal, which will not map to the MEMS columns properly. If we would like to keep this design, we will have to use one spherical mirror for each output position to re-image the beams onto the desired MEMS locations.

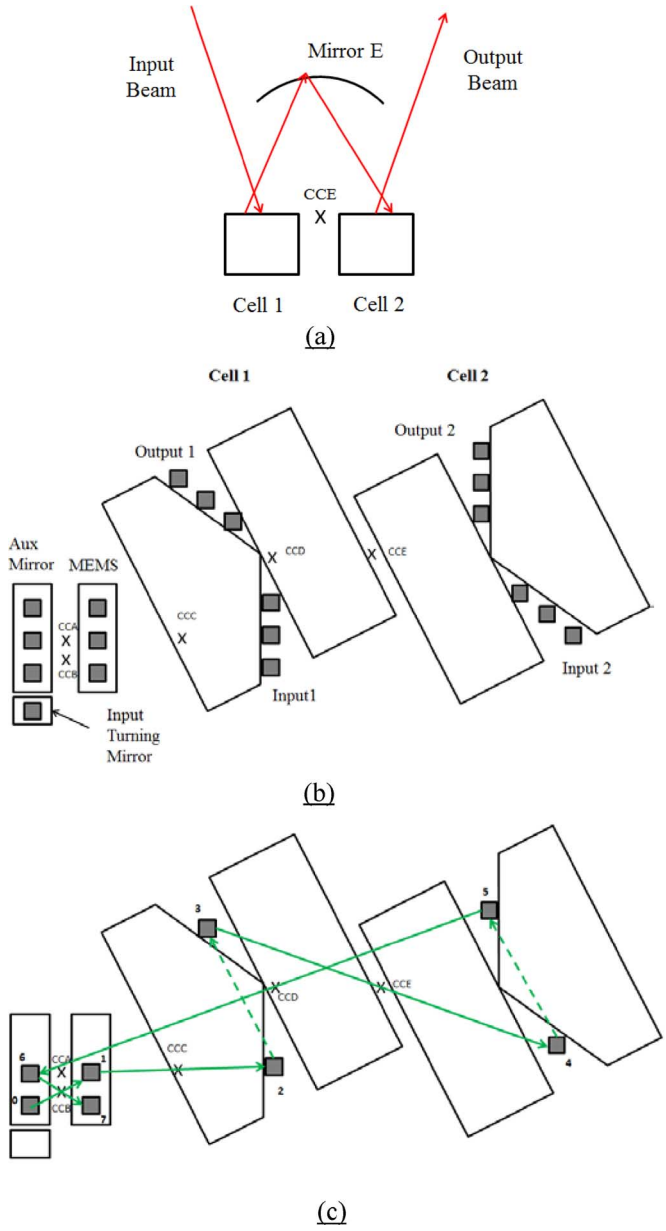

Fig. 10. (a) Top view of the dual Robert cell system coupled with mirror E used as a delay plane. (b) The structure of the coupled Robert cell showing all the possible beam spots. (c) The trajectory of a beam if it were to be sent into the delay plane.

The addition of many spherical mirrors can make the system somewhat cumbersome. A better solution is coupling two Robert cells using the integer-swirl design in Fig. 6(a) (as opposed to coupling two half-integer-swirl designs as in Figs. 6(b) and 8), using a spherical mirror E. The new design's top-view schematic is shown in Fig. 10(a), and its front view with Mirror E's center of curvature is shown in Fig. 10(b). When an array of input beams is sent into an input location of Cell 1, mirror E images the output beams of Cell 1 onto the corresponding input location of Cell 2. Fig. 10(b) demonstrates that the line connecting the output locations of the second cell is parallel to the line connecting the input locations. This makes it possible to use spherical mirror D to send the beams to the auxiliary

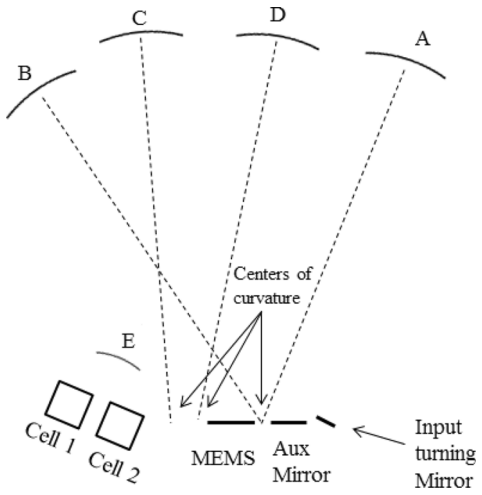

Fig. 11. Top view of a White-cell-based TTD device that uses the Robert cell as its delay plane.

mirror and then back onto the next column of the MEMS. Fig. 10(c) provides one example of the spot patterns formed in the case where the beams are switched into the delay plane by the MEMS. The indices 0 through 7 show the order of the spot locations. At the end of step 7, the output beams from the coupled Robert cell system are imaged onto the next column of the MEMS as desired.

When the Robert cells are integrated into the White cell, they are placed at the delay plane location as seen in Fig. 11. As a set of beams is selected to be delayed, the MEMS can reflect the beams onto mirror C, which sends the beams into the first Robert cell. The beams eventually come out of the second Robert cell, whereupon they diverge onto mirror D, which focuses the beams back onto the next row or column of the MEMS.

During the nth cycle of the binary White cell, while a traditional delay plane produces a delay that is proportional to 2^n, the Robert cell provides a delay proportional to n. Thus, over n cycles of operations with the smallest time increment Δ, the maximum achievable time delay for the Robert cell, $[n(n+1)/2]\Delta$, much similar to a quadratic White cell [10].

One potential source for concern would be the accumulation of aberrations over potentially hundreds of bounces. To minimize the aberrations (specifically astigmatism due to beams striking spherical mirrors at varying angles), two solutions present themselves. One option is to keep the angles of incidence small, which means lengthening the cell. While this also reduces the total number of bounces for a given delay, and thus further reduces aberration, it has to be traded off against the larger overall size. Another potential solution is to use toroidal mirrors to correct for astigmatism. The use of astigmatic mirrors in a Herriot cell will perturb the spot pattern [11]; probably the degree of astigmatism needed to correct the aberration due to off-axis beams is small enough not to affect the spot placement significantly, but would have to be accounted for during the design process. In previous work with White cells [3], a path containing 40 mirror reflections had very little loss due to aberration, using a combination of these two approaches (f# $>$ 10 and very slightly toroidal mirrors).

V. Summary

In this paper, we have discussed the way by which the Robert cell can be used as delay elements for existing optical TTD systems. We first reviewed the structure of the Robert cell, which is a three-mirror-system that allows light to experience multiple reflections and travel a long distance compared to its physical dimensions. Through ray matrix and difference equation analyses, we have derived the spot patterns and the properties of the Robert cell, allowing us to design variations of the Robert cell as the delay element for the White cell-based TTD system with the Binary cell structure. Compared to traditional delay elements such as glass blocks, lens trains, and optical fibers, the Robert cell is not only compact, but it can also achieve long time delays with low loss. Furthermore, ultra-long delays on the order of 100 ns can be attained using a coupled Robert cell design.

References

[1] B. L. Anderson, S. A. Collins, Jr., C. A. Klein, E. A. Beecher, and S. B. Brown, "Photonically produced true-time delays for phased antenna arrays," *Appl. Opt.*, vol. 36, no. 32, pp. 8493–8503, 1997.

[2] H. Zmuda and E. N. Toughlian, "Photonic aspects of modern radar," in *The Artech House Optoelectronics Library*, B. Culshaw, A. Rogers, and H. Taylor, Eds. Norwood, MA: Artech House, 1994.

[3] B. L. Anderson, J. G. Ho, W. D. Cowan, O. Blum-Spahn, A. Y. Yi, D. J. Rowe, M. R. Flannery, D. L. McCray, P. Chen, and D. J. Rabb, "Hardware demonstration of extremely compact optical true time delay device for wideband electronically steered antennas," *J. Lightw. Technol.*, vol. 29, no. 9, pp. 1343–1353, May 2011.

[4] B. L. Anderson, D. J. Rabb, C. M. Warnky, and F. M. Abou-Galala, "Binary optical true time delay based on the white cell: Design and demonstration," *J. Lightw. Technol.*, vol. 24, no. 4, pp. 1886–1895, Apr. 2006.

[5] S. Kunathikom, B. L. Anderson, and S. A. Collins, Jr., "Design of delay elements in binary optical true-time delay devices," *Appl. Opt.*, vol. 42, no. 35, pp. 6984–6994, Dec. 2003.

[6] C. Robert, "Simple, stable, and compact multiple-reflection optical cell for very long optical paths," *Appl. Opt.*, vol. 46, no. 22, pp. 5408–5418, Aug. 2007.

[7] J. White, "Long optical paths of large aperture," *J. Opt. Soc. Amer.*, vol. 32, no. 2, pp. 285–288, May 1942.

[8] D. Heriott, H. Kogelnik, and R. Kompfner, "Off-axis paths in spherical mirror interferometers," *Appl. Opt.*, vol. 3, no. 4, pp. 523–526, Apr. 1964.

[9] C. G. Tarsitano and C. R. Webster, "Multilaser Herriott cell for planetary tunable laser spectrometers," *Appl. Opt.*, vol. 46, pp. 6923–6935, 2007.

[10] B. L. Anderson and C. D. Liddle, "Optical true-time delay for phased array antennas: Demonstration of a quadratic White cell," *Appl. Opt.*, vol. 41, no. 23, pp. 4912–4921, 2002.

[11] D. R. Herriott and H. J. Schulte, "Folded optical delay lines," *Appl. Opt.*, vol. 4, no. 8, pp. 883–889, 1965.

Yu Shi is currently working toward the B.S. degree in electrical engineering at The Ohio State University, Columbus, OH, USA.

Betty Lise Anderson (M'78–SM'93) received the B.S.E.E. degree from Syracuse University, Syracuse, NY, USA, in 1978, and the M.S. and Ph.D. degrees in electrical engineering and materials science from the University of Vermont, Burlington, VT, USA, in 1987 and 1990, respectively.

She was Component Engineer for Flat Panel Displays at Tektronix from 1987 to 1989, then joined GTE Laboratories, Waltham, MA, USA, during 1980–84 as a Member of Technical Staff. She was also an MTS with C. S. Draper Labs, Cambridge, MA, USA, from 1984 to 1986.

Dr. Anderson is a senior member of the Optical Society of America and a member of the International Society of Optical Engineers and the American Society for Engineering Education. She was an associate editor for the IEEE Journal of Quantum Electronics from 2004 to 2009. She was the recipient of the *Outstanding Woman in Technology Award* from TechColumbus in 2005.